IEEE Access
Multidisciplinary | Rapid Review | Open Access Journal

Received April 18, 2019, accepted April 29, 2019, date of publication May 10, 2019, date of current version July 1, 2019.

Digital Object Identifier 10.1109/ACCESS.2019.2916072

A Collaborative Fuzzy Control Strategy of Aggregated Regenerative Electric Heaters for Real-Time Energy Balance in Micro-Grid

TING HUANG, YI SUN, BIN LI, AND JIANHONG HAO
School of Electrical and Electronic Engineering, North China Electric Power University, Beijing 102206, China
Corresponding author: Bin Li (18500777272@163.com)

This work was supported by the National Natural Science Foundation of China under Grant 51777068.

ABSTRACT As more and more renewable generation resources such as photovoltaic and wind-power are connected to the micro-grid in smart grid, it is prone to bring challenges to balance supply and demand for the uncertain and variable nature of renewable generation resources. In this paper, we propose a collaborative fuzzy control strategy (CFCS) of aggregated regenerative electric heaters (REHs) to balance renewable energy generation and maintain the real-time balance between supply and demand. First, we describe the system architecture of aggregated REHs for accommodating renewable energy. Then, we establish the information control model of a single REH. Next, based on the system architecture and the model, a collaborative control strategy, including state awareness, real-time analysis, scientific decision-making, and precise execution, is presented to realize the optimal control of the aggregated REHs for accommodating renewable energy. Finally, the simulation results show that the proposed strategy not only can meet the demand for accommodating renewable energy generation effectively but also ensure residential comfort and the heat-storage percent of REHs.

INDEX TERMS Renewable energy accommodation, regenerative electric heater, fuzzy algorithm.

NOMENCLATURE

Abbreviation	
CFCS	collaborative fuzzy control strategy
REH	regenerative electric heater phase
PCM	change material demand side
DSM	management thermostatically
TCL	controlled load

INDICES

i	index for time slot
k	index for REHs
j	index for evaluation indicators
l	index for column of matrix
min	lower limit of the heat-storage percent
max	upper limit of the heat-storage percent

PARAMETERS

s	the final operating status, which includes the heating state s_1, the heat-storage state s_2 the heat-exothermic state s_3, and the closed state s_4
T_{set}	temperature set-point by the resident ($^\circ C$)
DT	thermal insulation temperature dead band ($^\circ C$)
η	efficiency factor for REHs
Δt	length of a time slot i
r	generative heat flux density of the phase change material $J/m^2 \cdot s$
e	exothermic heat flux density of the phase change material $J/m^2 \cdot s$
S_1	area of the phase change material (m^2)
C	specific heat capacity of air ($KJ/(kg \cdot K)$)
h	convective heat transfer coefficient between the indoor air and the interior wall ($W/(m^2 \cdot K)$)
ρ	density of air ($kg/(m^3)$)
S_2	area of the interior wall (m^2)
L	width of the interior wall (m)
V	volume of the house (m^3)

The associate editor coordinating the review of this manuscript and approving it for publication was Ramazan Bayindir.

λ	thermal conductivity between the interior wall and the outdoor air $(W/(m \cdot K))$
M	heat-storage amount in the phase change material (J)
n	the amount of the REHs
m	the amount of the columns in the matrix
d^+	fuzzy positive ideal distance
d^-	fuzzy negative ideal distance
μ	membership degree of REHs
q	digital serial number of REHs
P	rated power of REHs (kW)
Q	priority queue of aggregated REHs
ID	the serial number of REHs chosen to be on
$\mathbf{F}$	matrix of triangular fuzzy values
$\mathbf{R}$	matrix of normalized fuzzy indicators
$\mathbf{D}$	matrix of fuzzy decision indicators
$\mathbf{M}^+$	matrix of fuzzy positive ideal values
$\mathbf{M}^-$	matrix of fuzzy negative ideal values
$\mathbf{W}$	matrix of weight vectors
$\mathbf{E}$	selected group of REHs

VARIABLES

sig	external control signal
S_n	operating status if not receiving $sin(i)$
T	indoor temperature $°C$
α	heat-storage percent of a REH
$T_w(i)$	temperature of the interior wall $°C$
$T_o(i)$	outdoor temperature at the start of time slot i $°C$
$action$	the on/off of REHs
P_{target}	accommodation target from the cloud-based platform (kW)

I. INTRODUCTION

The large consumption of energy further intensifies the resource shortage in smart grid [1]. The concerns on environment protection and renewable clean energy generation have driven the need to accommodate the renewable energy in a more efficient way [2], [3]. As a critical part of smart grid, micro-grid is an effective mode to accommodate renewable energy locally and promote sustainable development, formed by distributed energy resource, energy storage devices, and loads of local buildings in a certain area [4]–[6]. However, one main challenge is on balancing renewable energy generation with the intermittent, uncertainty, and variable nature in the micro-grid. Currently, the elasticity of loads on the demand-side has offered an opportunity to improve the renewable energy accommodation and reduce the abandoned energy effectively in smart grid [7]–[9].

Among all residential loads in a grid-connected smart home system, phase-change-type aggregated regenerative electric heaters (REHs) are good candidates for load regulation. The reasons are mainly based on the following fours aspects. First, REHs can store electric energy by heating phase change material (PCM) [10]. Second, the REH is a pollution-free environmental-friendly load and aggregated REHs have a large adjustable capacity for their high penetration rate and enormous number at residential side [11]. Third, the REH equipment has realized the integration of perception, calculation, control, and communication function, which is advantageous to realize automatic control [12]. Fourth, PCM have the advantages of constant temperature and high heat-storage density [13].

In the literatures, there have many relevant studies on demand side management (DSM). DSM is a core technique to balance real-time energy in supply and demand by controlling and optimizing residential energy consumption [14]. There are two methods to model several main thermostatically controlled loads (TCLs) in demand side, which are established based on the physical characteristics ([15], [16]) and the equivalent thermodynamic parameters (ETP) ([17]–[19]). In [20], a thermostatically controlled model and an adaptive self-adjusting control system of electric heaters in the heating stage were proposed. Besides, storing energy loads were also proved to be effective to reduce energy consumption and achieve zero energy buildings [21]. The building envelope with PCMs was also validated to ensure indoors thermal environment by using less energy [22]. In [23]–[25], Smoothing out the renewable energy generation by regulating energy storage system was investigated. In [26]–[28], the authors demonstrated that energy storage system contributed to improve reliability and stability of renewable energy resources was studied. In [10], the operational principle of REHs was introduced and the multiple measurement parameters were analyzed, an accurate model of REH is not presented.

On the other hand, control strategies are also necessary to manage and optimize the energy consumption. Based on different control mechanism for TCLs, the control strategies could be divided into three categories: switching status control ([29]), thermostat setpoint control ([30]–[34]), and voltage control ([35], [36]). In [37], the authors presented three schemes to regulate the loads systematically, which was proved that it can reduce 23% of the power consumption. In [38], the authors introduced a real-time two-stage optimization model for multiple TCLs to smooth the power fluctuation in a distribution network, and the strategy evaluated the load regulation capacity, also made the target demand curves for each load group economically. Therefore, in these studies, the optimal management of thermostatically controlled loads has been investigated to accommodate the renewable energy efficiently.

However, the model and control strategy for REHs suffer from several following drawbacks in the above researches, which have been addressed in this paper:

1) The existing models of TCLs failed to reflect the physical characteristics of REHs accurately, due to REHs also possess behavior of energy storage, e.g. [14]–[17],
2) Some simplified models of aggregated REHs only considered the fluctuation of power consumption, which

limits the application scope of these models in load regulations, e.g. [39], [40],

3) Some strategies for TCLs focused on the comfort of indoor temperature. With the lack of consideration for heat-storage percent, these strategies are unsuitable to control REHs, e.g. [27], [28],
4) Some strategies aimed at smoothing power and balancing the energy, which results in the loss of residential comfort and fairness, e.g. [23], [24].

In addition, the fuzzy logic control is a widely applied control method for engineering control [41], [42]. First, it can simplify the complexity of system design, especially for the control of non-linear, time-varying systems. Second, it does not depend on the precise mathematical model of the controlled object, which can make up tiny differences in equipment. Third, it has better robustness, adaptability and fault tolerance. In [43], the authors proposed a voltage control method based on fuzzy control to accomplish energy management. Some researches applied fuzzy controls to microgrid operations, such as controlling distributed generations and power point tracking of a photovoltaic system [44]–[47]. The results demonstrated that fuzzy algorithm can improve the stability and accuracy effectively and achieve optimal control by considering multiple index values comprehensively.

In contrast to the existing studies mentioned above, we establish a model that can accurately reflect the operating characteristics of a single REH and propose a collaborative fuzzy control strategy (CFCS) based on the perceived valid data and the compromised fuzzy multi-attribute decision-making algorithm, which considers both room temperature and heat-storage percent for the aggregated REHs. The proposed strategy includes four steps: state awareness, real-time analysis, scientific decision-making, and precise execution to realize optimal resource allocations.

The contributions of this paper are twofold. First, we establish a single REH information control model, which can reflect the actual operating characteristics and provide a foundation for accuracy and optimal control of REHs. Second, based on the proposed model and fuzzy algorithm, we propose a collaborative control strategy for aggregated REHs. The strategy can realize the real-time power balance and improve energy efficiency by optimize the control of the operating statuses for micro-grid. Besides, the strategy can ensure comfort and the heat-storage percent of REHs for residents.

The rest of this paper is organized as follows: Section II introduces the system architecture of aggregated REHs to accommodate renewable energy in the micro-grid. Section III describes the information control model of a single REH proposed in this paper. The collaborative control strategy based on fuzzy algorithm is presented in Section IV. The simulation results and analysis are covered in Section V to demonstrate the effectiveness of the strategy. The conclusions are presented in Section VI.

II. SYSTEM ARCHITECTURE

Fig.1 shows a system architecture of aggregated REHs to balance real-time renewable energy generation in a community-based micro-grid.

As shown in the Fig.1, there are lots of load aggregators (LA) to participate in the demand response program in the architecture, which present a link between smart grid and residents [48]–[50]. For residents, LAs sign agreements with residents participating in demand response programs, so the cloud-based platforms can collect and analyze real-time measurement parameters and residential intentions. For smart grid, in real-time market (RTM) [51], when power control center receives and forwards the signals to LAs that require to balance renewable energy generation, all LAs immediately assess its potential to decide whether to participate in this demand response program based on the collected information, then upload the decision to power control center. Therefore, the power control center can select the proper LA to participate in this program according the competition strategy [52], [53]. Also, the control center assigns the target response to each selected LA based on their accommodated ability. Last, the selected LAs generate and send control signals to the REHs by executing a control strategy, which will be proposed in Section IV. The signals are implemented by local REHs based on the interior operating logic. Through the above mechanism, the goal of balancing the renewable energy generation is achieved.

Before introducing the control strategy, we introduce the related information control model of a single REH in Section III to describe the interior operating logic.

III. INFORMATION CONTROL MODEL OF REH

The structure of REH includes electric heating pieces, thermal storage tank, axial flow fans, ventilation, and temperature controller. The REH extracts the indoor air through the axial flow fans. Then, the air is heated by flowing through the electric heating pieces. Next, the heated air is discharged from the ventilation. By the above processes, an indoor air circulation is completed [10]. In the operating process, the operating statuses of a REH is divided into four states: heating, heat-storage, heat-exothermic, and closed. Fig.2 shows the temperature evolution and heat-storage percent evolution in these four operating statuses.

The information control model of a single REH includes operating status control model, temperature evolution model, and heat-storage percent evolution model. As shown in Fig.3. It reflects the relationship between the indoor temperature and operating statuses as well as external signals and the heat-storage percent.

The operating status control model of a single REH is described as follows:

$$s(i) = \begin{cases} sig(i), & if\ receiving\ \mathrm{sig}(i) \\ s_n, & if\ not\ receiving\ sig(i) \end{cases} \quad (1)$$

where s(i) denotes the operating status in time slot i; sig(i) denotes the external control signal at the start of time slot i,

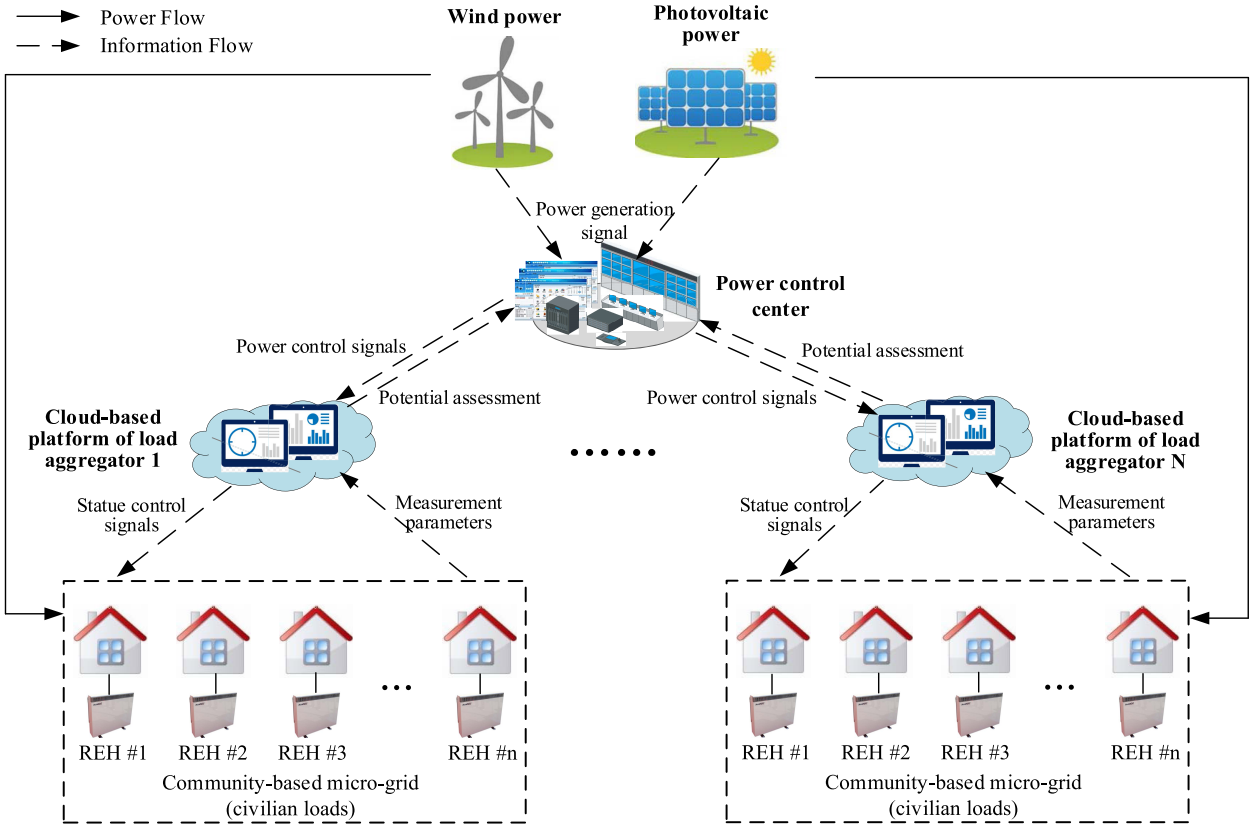

FIGURE 1. System architecture to accommodate renewable energy.

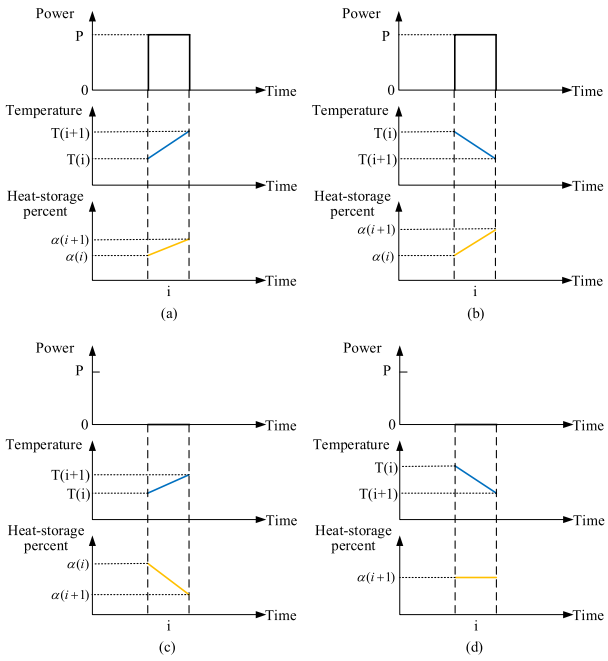

FIGURE 2. Schematic diagram of temperature evolution and heat-storage percent evolution in four operating statuses. (a) Heating state. (b) Heat-storage percent. (c) Heat-exothermic. (d) Closed state.

the value includes s_1, s_2, s_3, and s_4, s_1 denotes the heating state, s_2 denotes the heat-storage state, s_3 denotes the heat-exothermic state, s_4 denotes the closed state; s_n denotes an operating status if not receiving $sig(i)$, it is determined by Fig.4. In Fig.4, $T(i)$ denotes the indoor temperature at the start of time slot i; $\alpha(i)$ is the heat-storage percent of a REH at the start of time slot i.

Based on the energy conservation law, the indoor temperature evolution model and heat-storage percent evolution model are established.

The indoor temperature evolution model is described in (2), as shown at the bottom of the next page, which describes the change of indoor temperature under different operating statuses. where $T_w(i)$ is temperature of the interior wall at the start of time slot i; $T_o(i)$ is the outdoor temperature at the start of time slot i.

The heat-storage percent evolution model is described in (3), which describes the change of the heat-storage percent under different operating statuses.

$$\alpha(i+1) = \begin{cases} \alpha(i) + \dfrac{rS_1\Delta t}{M}, & s(i) = s_1 \\ \alpha(i) + \dfrac{\eta P \Delta t}{M}, & s(i) = s_2 \\ \alpha(i) - \dfrac{eS_1\Delta t}{M}, & s(i) = s_3 \\ \alpha(i), & s(i) = s_4 \end{cases} \tag{3}$$

IV. CFCS

This section presents a collaborative fuzzy control strategy of aggregated REHs to generate control signals in Section II,

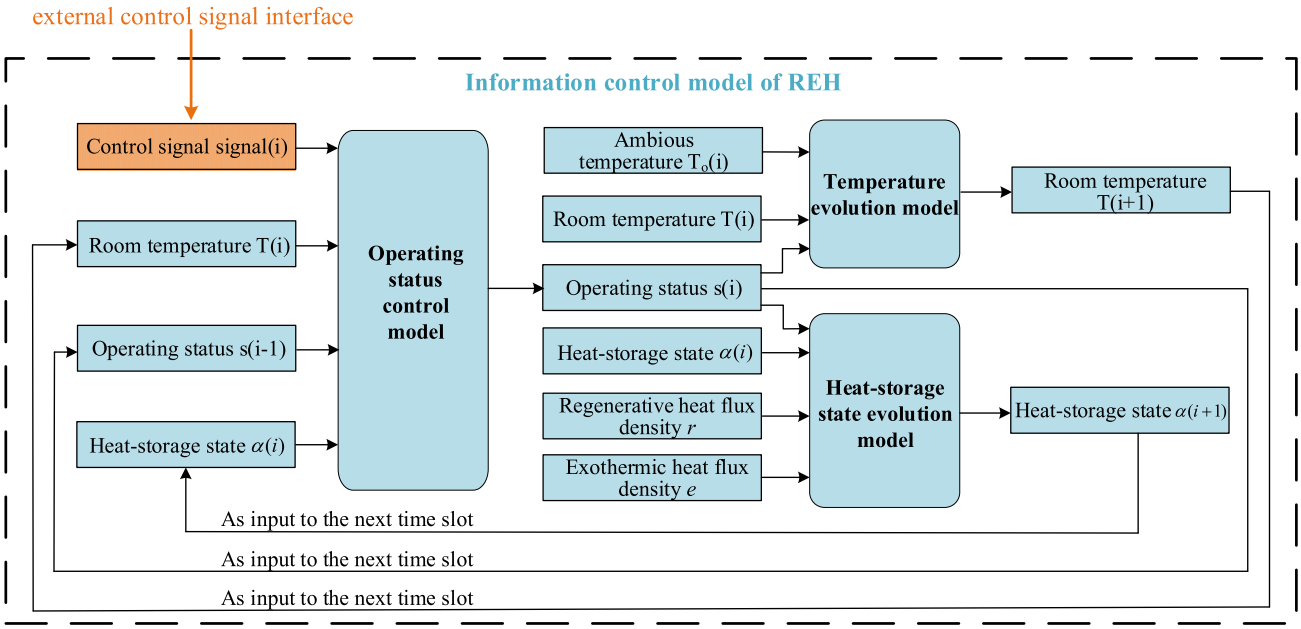

FIGURE 3. Schematic diagram of the information control model.

based on the model developed in Section III. As shown in the Fig.5, the proposed control strategy includes four parts: state awareness, real-time analysis, scientific decision-making, and precise execution. The implementation logics of these four parts are designed as shown in Fig.5.

A. STATE AWARENESS LOGIC

State awareness logic is used to obtain real-time measurement parameters of each REH k. The measurement parameters include the indoor air temperature $T_k(i)$, the interior wall temperature $T_{w,k}(i)$, the ambient temperature $T_{o,k}(i)$, and the heat-storage percent $\alpha_k(i)$ of the REH k.

B. REAL-TIME ANALYSIS LOGIC

In the real-time analysis, the heat-storage percent $\alpha_k(i)$ and indoor temperature $T_k(i)$ are considered as evaluation indicators to form a priority queue of aggregated REHs, based on the eclectic fuzzy multi-attribute decision-making algorithm. Particularly, the greater the membership degree in the queue is, the better the index value is, and the REH is more likely selected to be turned off in the queue.

The basic steps forming a priority queue of aggregated REHs are as follows:

Step 1: Convert each REH data to triangular fuzzy values. Indoor air temperature $T_k(i)$ is taken as an example, $\mathbf{F}(\mathrm{R})$ is the overall fuzzy set in set of real number R, and f_{kj} represents the triangular fuzzy value of the evaluation indicator j of the REH k in $\mathbf{F}(\mathrm{R})$ ($j = 1, 2; k = 1, 2, \ldots, n$). The triangular fuzzy value of the indoor air temperature $T_k(i)$ is expressed as follows:

$$f_{kj} = (T_k(i), T_k(i), T_k(i)) \tag{4}$$

After all the data is completely converted into triangular fuzzy values, the fuzzy indicator matrix $\mathbf{F} = (f_{kj})_{n\times m}$ is formed.

In addition, the weight vectors of two indicators are given in quantitative form, which are described as follows:

$$\begin{aligned} W &= [W_1, W_2, \cdots, W_j] \\ &= [(w_1, w_1, w_1), (w_2, w_2, w_2), \cdots, (w_j, w_j, w_j)] \end{aligned} \tag{5}$$

Step 2: Normalize the fuzzy indicator matrix $\mathbf{F}$. For each evaluation indicator j, the fuzzy index values of REH k is $f_{kj} = (a_{kj}, b_{kj}, c_{kj})$ in F.

$$T(i+1) = \begin{cases} T(i) + \dfrac{\eta P\Delta t - r\Delta t S_1 - hS_2(T(i) - T_W(i))\Delta t - \lambda L(T_W(i) - T_o(i))\Delta t}{C\rho V}, & s(i) = s_1 \\ T(i) - \dfrac{hS_2(T(i) - T_W(i))\Delta t + \lambda L(T_W(i) - T_o(i))\Delta t}{C\rho V}, & s(i) = s_2 \\ T(i) + \dfrac{e\Delta t S_1 - hS_2(T(i) - T_W(i))\Delta t - \lambda L(T_W(i) - T_o(i))\Delta t}{C\rho V}, & s(i) = s_3 \\ T(i) - \dfrac{hS_2(T(i) - T_W(i))\Delta t + \lambda L(T_W(i) - T_o(i))\Delta t}{C\rho V}, & s(i) = s_4 \end{cases} \tag{2}$$

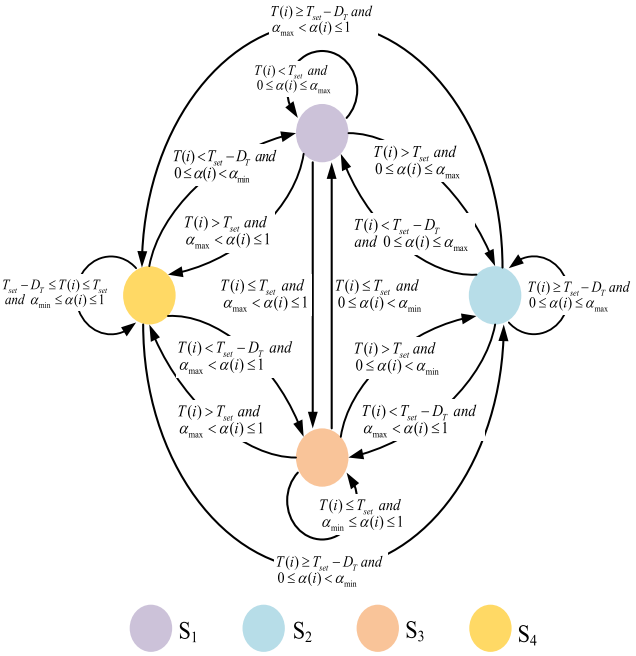

FIGURE 4. State transition diagram if not receiving sig(i).

The normalized fuzzy indicator matrix $\mathbf{R}$ is described as follows:

$$\mathbf{R} = (r_{kj})_{n\times m} = \begin{bmatrix} r_{11}, \cdots, r_{1j}, \cdots \\ \vdots \\ r_{k1}, \cdots, r_{kj}, \cdots \\ \vdots \\ r_{n1}, \cdots, r_{nj}, \cdots \end{bmatrix} \tag{6}$$

where r_{kj} is expressed as follows:

$$r_{kj} = \left(\frac{a_{kj}}{\max(c_{kj})}, \frac{b_{kj}}{\max(b_{kj})}, \min\left(\frac{c_{kj}}{\max(a_{kj})}, 1\right)\right) \tag{7}$$

Step 3: Construct the fuzzy decision matrix $\mathbf{D}$. It is formed by weighting the normalized fuzzy indicator matrix $\mathbf{R}$, and it is described as follows:

$$\mathbf{D} = \mathbf{W}\Theta\mathbf{R} = (d_{kj})_{n\times m} = \begin{bmatrix} d_{11}, \cdots, d_{1j}, \cdots \\ \vdots \\ d_{k1}, \cdots, d_{kj}, \cdots \\ \vdots \\ d_{n1}, \cdots, d_{nj}, \cdots \end{bmatrix} \tag{8}$$

where $d_{kj} = W_j * r_{kj}$.

Step 4: Determine the fuzzy positive ideal value $\mathbf{M}^+$ and the fuzzy negative ideal value $\mathbf{M}^-$. $\mathbf{M}^+$ and $\mathbf{M}^-$ are defined as follows:

$$\begin{aligned} \mathbf{M}^+ &= (M_1^+, M_2^+, \cdots, M_m^+) \\ \mathbf{M}^- &= (M_1^-, M_2^-, \cdots, M_m^-) \end{aligned} \tag{9}$$

where $M_l^+ = \max(d_{1l}, d_{2l}, \cdots, d_{nl})$,which represents the fuzzy maximum value corresponding to the fuzzy index value of the column l in $\mathbf{D}$; $M_l^- = \max(d_{1l}, d_{2l}, \cdots, d_{nl})$, which represents the fuzzy minimum value corresponding to the fuzzy index value of the column l in $\mathbf{D}$.

Step 5: Calculate the distance d_k^+ between the d_{kl} of the REH k and the fuzzy positive ideal value M_l^+, the distance d_k^- between the d_{kl} of the REH k and the fuzzy negative ideal value M_l^-. d_k^+ and d_k^- are defined as follows:

$$\begin{aligned} d_k^+ &= \sqrt{\sum_{l=1}^{m}(d_{kl} - M_l^+)^2} \\ d_k^- &= \sqrt{\sum_{l=1}^{m}(d_{kl} - M_l^-)^2} \end{aligned} \tag{10}$$

Step 6: Calculate the membership degree μ_k of the REH k. The membership degree μ_k is described as follows:

$$\mu_k = \frac{d_k^-}{d_k^- + d_k^+} \tag{11}$$

Obviously $0 \leq \mu_k \leq 1$, and if the indicator value r_{kl} of the REH k is closer to M_l^+, the μ_k will be closer to 1.

Step 7: Sort the membership degrees μ_k. The smaller the μ_k is, the lower the index of the REH k is, and the higher probability of being selected for the REH k to be turned on is. As shown in the Fig.6, the priority queue $Q(i)$ of aggregated REHs is generated.

C. SCIENTIFIC DECISION-MAKING LOGIC

Scientific decision-making determines the load groups $\mathbf{E}_1(i)$ and $\mathbf{E}_2(i)$ to generate the control signals according to different control rules. The combinatorial logic is as follows:

Step 1: Select the front q REHs from the current selection REH priority queue $Q(i)$ and form a load group $\mathbf{E}_1(i) = \{Q_k(i)|k = 1, 2, \cdots, q\}$, as shown in the Fig.7. The selected REHs meet the following constraints, the fluctuation range is in the rated power of one REH:

$$P_{target}(i) - \frac{P}{2} \leq \sum_{k=1}^{q} P \cdot action_k(i) \leq P_{target}(i) + \frac{P}{2} \tag{12}$$

where $action_k(i)$ represents the on/off of REH k in time slot i, and it is defined as follows:

$$action_k(i) = \begin{cases} 1, & s_k(i) = s_1 \text{ or } s_k(i) = s_2 \\ 0, & s_k(i) = s_3 \text{ or } s_k(i) = s_4 \end{cases} \tag{13}$$

Step 2:Other REHs in $Q(i)$ are selected to form a load group $\mathbf{E}_2(i) = \{Q_k(i)|k = q+1, q+2, \cdots, n\}$, as shown in the Fig.8:

D. PRECISE EXECUTION LOGIC

For each REH in the load group $\mathbf{E}_1(i)$ and $\mathbf{E}_2(i)$, precise execution logic generates the control signal, which is the executed operating status. The generation rules of $s_k(i)$ are described as follows:

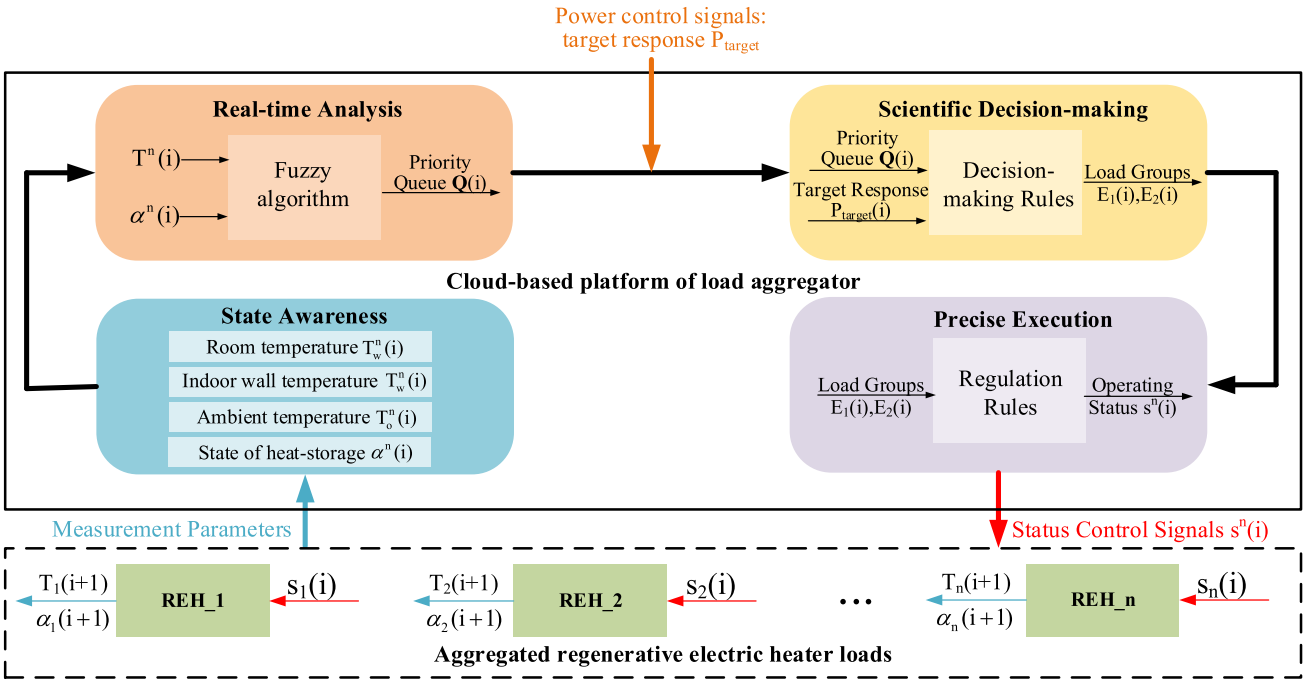

FIGURE 5. Implementation framework of the control strategy.

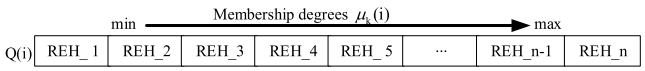

FIGURE 6. Schematic diagram of the REH priority queue.

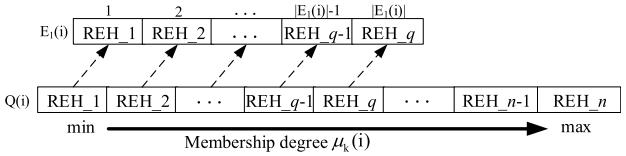

FIGURE 7. Schematic diagram of generating the REH group $\mathbf{E}_1(i)$.

1) For each REH k in the group $\mathbf{E}_1(i)$, the executed operating status $s_k(i)$ is described below:

$$s_k(i) = \begin{cases} s_1, & T_k < T_{set} - D_T \text{ and } 0 \le \alpha_k(i) < \alpha_{\max} \\ s_2, & T_k \ge T_{set} - D_T \text{ and } 0 \le \alpha_k(i) < \alpha_{\max} \\ s_3, & T_k \le T_{set} \text{ and } \alpha_{\max} < \alpha_k(i) \le 1 \\ s_4, & T_k > T_{set} \text{ and } \alpha_{\max} < \alpha_k(i) \le 1 \end{cases} \tag{14}$$

2) For each REH k in the group $\mathbf{E}_2(i)$, the executed operating status $s_k(i)$ is described below:

$$s_k(i) = \begin{cases} s_3, & T_k(i) < T_{set} - D_T \text{ and } \alpha_{\min} \le \alpha_k(i) \le 1 \\ s_4, & T_k(i) \ge T_{set} - D_T \text{ or} \\ & T_k(i) < T_{set} - D_T \text{ and } 0 \le \alpha_k(i) \le \alpha_{\min} \end{cases} \tag{15}$$

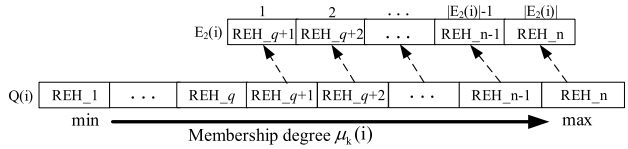

FIGURE 8. Schematic diagram of generating the REH group $\mathbf{E}_2(i)$.

E. DESCRIPTION OF CFCS

In this section, the implementation of CFCS for aggregated REHs at a time slot i is shown in the Fig.9. And the specific implementation are as follows:

Step 1:For each REH k, obtain relevant measurement parameters: $T_k(i)$, $T_{w,k}(i)$, $T_{o,k}(i)$,$\alpha_k(i)$;

Step 2: Calculate the membership degree $\mu_k(i)$ of each REH k at a time slot i, as defined in (4)-(11);

Step 3: For all REHs, form a priority sorting queue $\mathbf{Q}(i)$ according to $\mu_k(i)$ of each REH k;

Step 4: Form the group $\mathbf{E}_1(i)$ and $\mathbf{E}_2(i)$, as described in *IV-C*.

Step 5: For each REH k in $\mathbf{E}_2(i)$ and $\mathbf{E}_2(i)$, generate control signal $s_k(i)$, as defined in (14)-(15). And sends the control signal to each REH.

V. CASE STUDIES

To illustrate the performances of the proposed collaborative control strategy, simulations are conducted using MATLAB. It can solve large-scale optimization problems with convenient operation and efficient numerical calculation, which makes the parameter revision and scheme optimization more flexible.

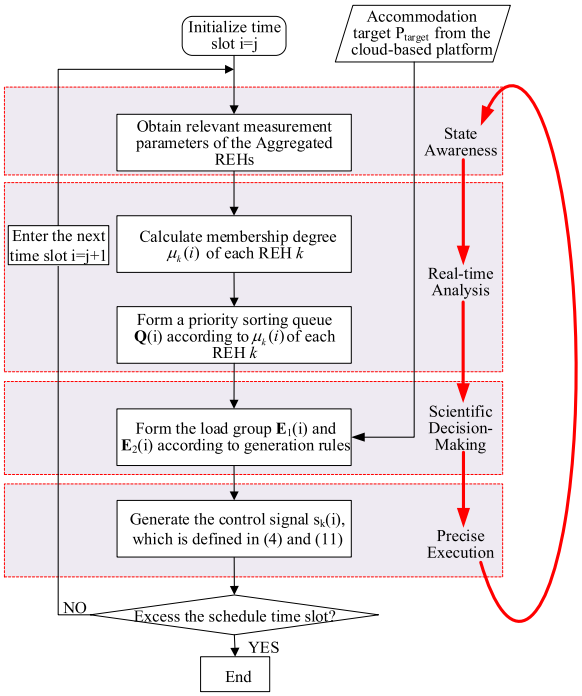

FIGURE 9. Implementation of the CFCS.

The first case is used to demonstrate the effectiveness and advantages of CFCS, which shows how the strategy schedules each resident with more detailed information in a five-REH system, then we compare the simulation results in a large-scale system between the proposed strategy and two contrast strategies (Contrast-1 and Contrast-2) in the same condition. Please note that, the contrast strategies quote the common control theory which is reflected in [33], [34], [39], and [54], [55]. The control theory applied state-queueing model to establish a state queueing and then control the status of TCLs, considering indoor temperature. On this basis, contrast-1 strategy takes in account heat-storage percent more, and contrast-2 strategy takes in account indoor temperature more.

The second case is designed to make recommendations to engineering applications, which analyzes the changes of average accommodation deviation, average temperature, and heat-storage percent with same target response and different numbers of REHs under CFCS.

A. SIMULATION PARAMETER CONFIGURATION

In the simple system of the first case, the number of the REHs is set to 5, and the simulation duration is 10 minutes. In the large system of the first case, the number of REHs in the large system is set to 1000, and the duration is 60 minutes.

In the second case, the numbers range of REHs from 200 to 2000, with 200 as an interval, the duration is 60 minutes. The initial status for the REHs are shown in Table 1. The physical parameters for the REHs are shown in Table 2, the length of each time slot is 1 minute. Note that, all parameters are the same for the two cases.

TABLE 1. The initial status for aggregated rehs [11].

Parameters	Value
The initial indoor temperature	Random dist. between 15-25℃
The initial heat-storage percent	Random dist. between 5%-95%
The outdoor temperature(winter)	Random dist. between 0-7℃
The comfortable temperature range	20~22℃
The comfortable heat-storage percent range	40%~70%

TABLE 2. Physical parameters for aggregated rehs [10], [11].

Parameters	Value	Parameters	Value
P	3.2	S_2	25
η	0.9	V	100
r	678.89	C	1.013
e	1243.10	ρ	1.164
S_1	1	h	8.7
α_{max}	95%	λ	0.45
α_{min}	5%	L	1

B. EFFECTIVENESS ANALYSIS

1) FIVE-REH SYSTEM

Based on the proposed model and strategy, the first system with five REHs is carried out to verify the effectiveness. The simulation results are shown in the Fig.10 and Table 3, which presents the status changes of every REH and parameter changes in each time slot.

It can be shown in the Fig.10 that in the first time slot, REH #1, #2, #3, #4 are ON to match the target response accurately while highest temperature and heat-storage percent of REH #5. In the second time slot, REH #1 is selected to be ON at heat-storage state to increase the heat-storage percent and REH #4 is also selected to be ON at heating state with lower heat-storage percent and indoor temperature, while REH #3 is at heat-exothermic state with higher heat-storage percent. Therefore, the heat-storage percent of REH #5 is constant and still highest while the highest temperature of REH #2 declined at the closed state.

Before the fifth time slot, REH #5 is selected to be OFF to match the target response and at closed state with highest heat-storage percent, which causes the temperature of REH #5 decrease to 19.92°. Therefore, the state is changed to the heat-exothermic state to increase the temperature, and the highest heat-storage percent decreases in the fifth time slot. In the eighth time slot, it is clear that REH #1, #3, and #4 with lower heat-storage percent are selected to be ON while there is little difference in temperature between REHs. However, the status of the selected REHs are at heat-storage state, so the temperature of REH #3 decreases to 19.74° and become the lowest temperature. Therefore, in ninth time slot, the state of REH #3 is changed to be at heating state to increase the

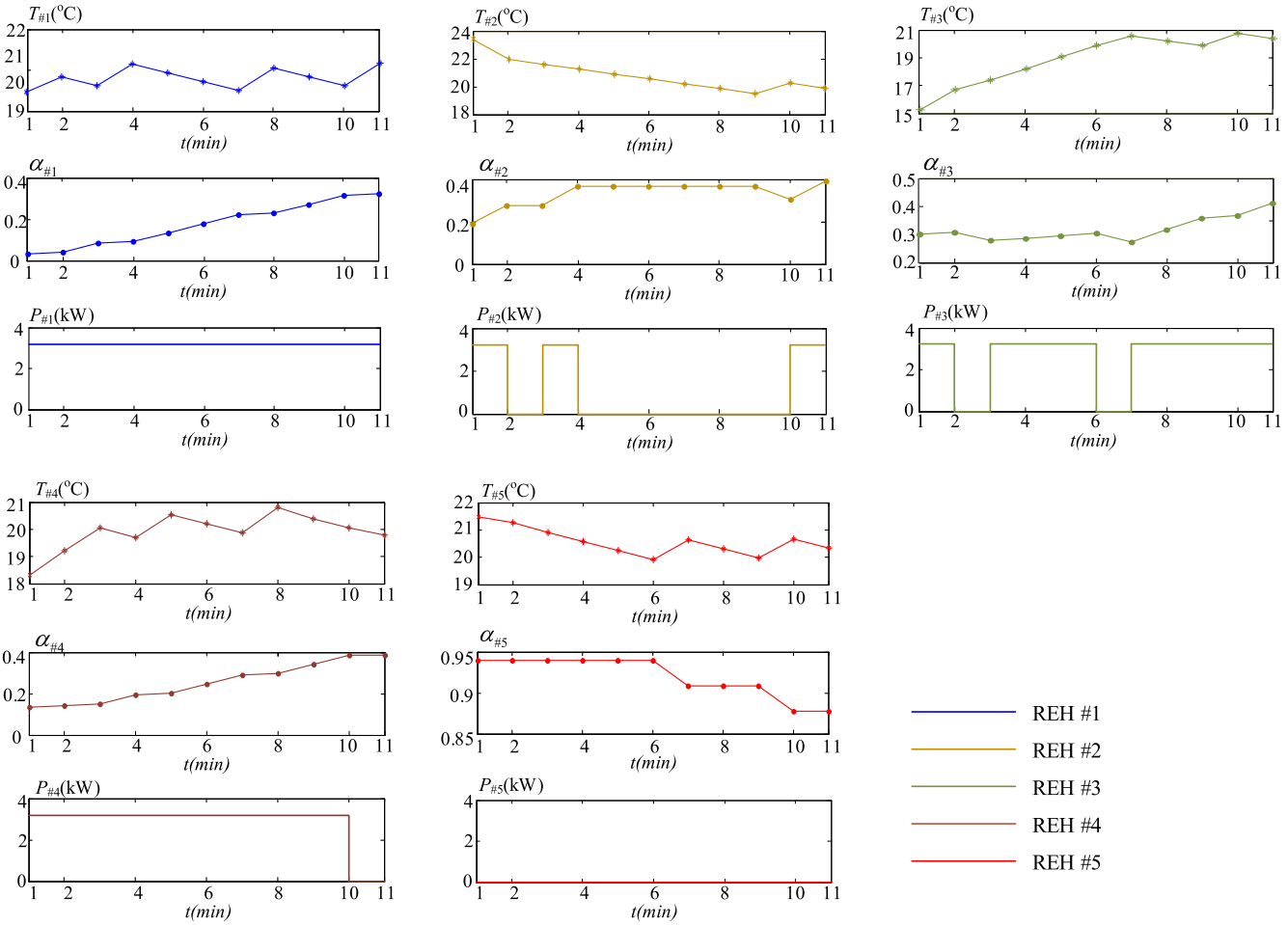

FIGURE 10. Simulation results of each REH in five-REH system.

temperature. Similarly, the temperature of REH #1 decreases to 19.92° and become the lowest temperature in this time slot. In the same time, the state of REH #5 changes to the heat-exothermic state from the closed state due to the decrease of temperature, so the highest heat-storage percent declined.

From the Table 3, the average deviation of system is 0.808kW, which is no more than a rated power, and the temperature gap is gradually reduced to 0.99 from 8.17 in the initial state, the heat-storage percent gap is also reduced from 0.91 to 0.56. The results show that the performance of the system will eventually tend to a stable and well-proportioned distribution, ensuring the fairness and comfort of all residents.

Based on the above analysis, the proposed control strategy is equitable and effective, which can achieve energy balance between demand and response, and an ideal tendency of indoor temperature and heat-storage percent.

TABLE 3. Simulation results in each time slot.

i	Deviation/kW	$T_{min}(i)$	$T_{max}(i)$	$\alpha(i)_{min}$	$\alpha(i)_{max}$	ID
0	—	15.25	23.42	0.03	0.94	—
1	1.13	16.67	22.07	0.04	0.94	1,2,3,4
2	0.34	17.38	21.74	0.08	0.94	1,4,
3	0.11	18.22	21.41	0.09	0.94	1,2,3,4
4	0.92	19.05	21.07	0.13	0.94	1,3,4
5	1.02	19.89	20.74	0.18	0.94	1,3,4
6	1.13	19.75	20.63	0.22	0.91	1,4
7	1.28	20.07	20.80	0.23	0.91	1,3,4
8	1.21	19.74	20.40	0.27	0.91	1,3,4
9	0.91	19.92	20.76	0.32	0.88	1,3,4
10	0.03	19.77	20.76	0.32	0.88	1,2,3,

2) LARGE SYSTEM

To confirm the advantages of the proposed strategy, a large system with 1000 REHs is designed, and we compare the different performances under three control strategies from three aspects.

Fig.11 compares the accommodation deviation under three strategies. From the Fig.11, we can observe that all strategies have a slight deviation. However, under the proposed strategy, the maximum deviation is 1.6kW, and the maximum deviation under contrast strategy is 2.8kW. It clearly shows the

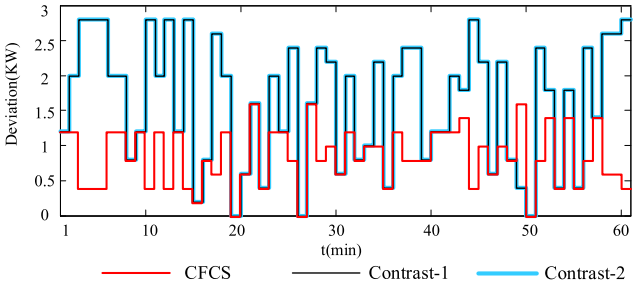

FIGURE 11. Accommodation deviation under three strategies.

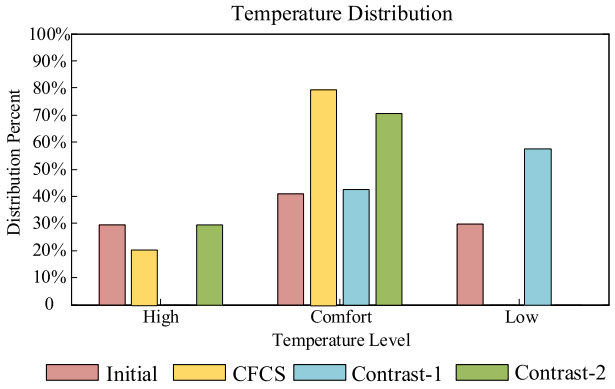

FIGURE 12. Comparison of temperature distribution.

smaller deviation of the proposed strategy, which proves the effectiveness of the proposed strategy.

For temperature distribution, we evaluate the performances under three strategies and the results are shown in the Fig.12. The indoor temperature is divided into three levels: high, comfort, low. The temperature of high level is higher than 22°, and the temperature range of comfort level is $20-22°$, the temperature of low level is lower than 20°. The heat-storage percent is divided into three levels: high, medium, low. The heat-storage percent of high level is 70%-100%, the heat-storage percent of medium level is 40%-70%, and the heat-storage percent of low level is 0%-40% [23].

Fig.12 compares the indoor temperature distribution of three strategies. We can observe that the percent of temperature in comfortable-level group under the proposed strategy is highest. All REHs are distributed in the high temperature group and comfortable temperature group under CFCS and Contrast-2. Under Contrast-1, all REHs are distributed in the comfortable group and low temperature group. Moreover, the percent of REHs in the comfortable range is 73.1% under CFCS while the percent is 70.6% under Contrast-2.

Obviously, the residential comfort under the proposed strategy is better than contrast strategies. Because constrats-1 focuses on the improvement of heat-storage percent, and the most energy is used for heating the storage unit, which causes the decline of temperature. And compared to contrast-2, under the proposed strategy, the REHs with lower temperature are selected preferentially, and it can avoid wasting energy by limiting the excessive rise of temperature.

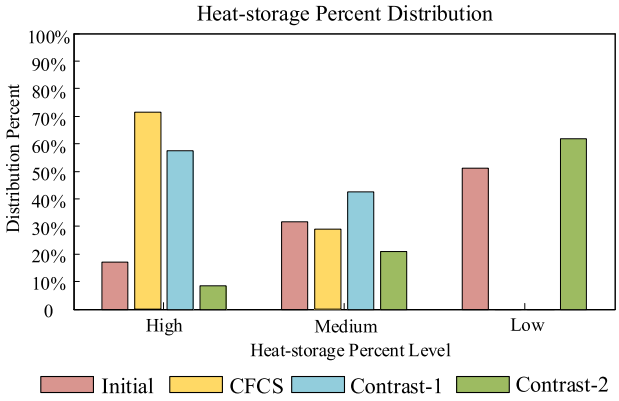

FIGURE 13. Comparison of heat-storage percent distribution.

For heat-storage percent distribution, we compare the different distributions under three strategies. From the Fig.13, we can observe that the percent of heat-storage percent in the high-level group under the proposed strategy is highest. All REHs are distributed in the high heat-storage percent group and medium heat-storage percent group under CFCS and Contrast-1, while the percent of REHs in low heat-storage percent group is 62% under Contrast-2. Obviously, the performance of heat-storage under Constrast-2 is worse.

Besides, the heat-storage percent of each resident in the high-level group under Contrast-1 is higher than it under the proposed strategy. The energy of Contrast-1 is used to further improve the heat-storage percent. On the contrary, the energy under the proposed strategy is used to increase the heat-storage percent of more loads to ensure fairness. Therefore, the percent of REHs in high heat-storage percent under Contrast-1 is lower than the percent of REHs under CFCS.

From the above analysis, the indoor temperature distribution and the heat-storage percent distribution under the proposed strategy are balanced and better. Because the Contrast-1 and Contrast-2 only consider one factor, and it will cause excessive increase of the factor and a poor distribution of the other factor.

C. PERFORMANCE ANALYSIS

This subsection analyzes the performances of the proposed strategy under a certain target response curve and various numbers of REHs to obtain an appropriate number range of REHs, which can provide references for demand-side resource distribution in the micro-grid.

From the Fig.14, we can observe that as the number of REHs n increases, average accommodation deviation decreases gradually and finally converges to 0, while average temperature and heat-storage percent rapidly decrease to a lower level after a steady state period.

When n is in [200,800], due to that the required energy for saturating heat-storage and thermal heating of all residents is smaller than target response for ever, all REHs are selected to be ON to bridge the gap, which creates higher temperature

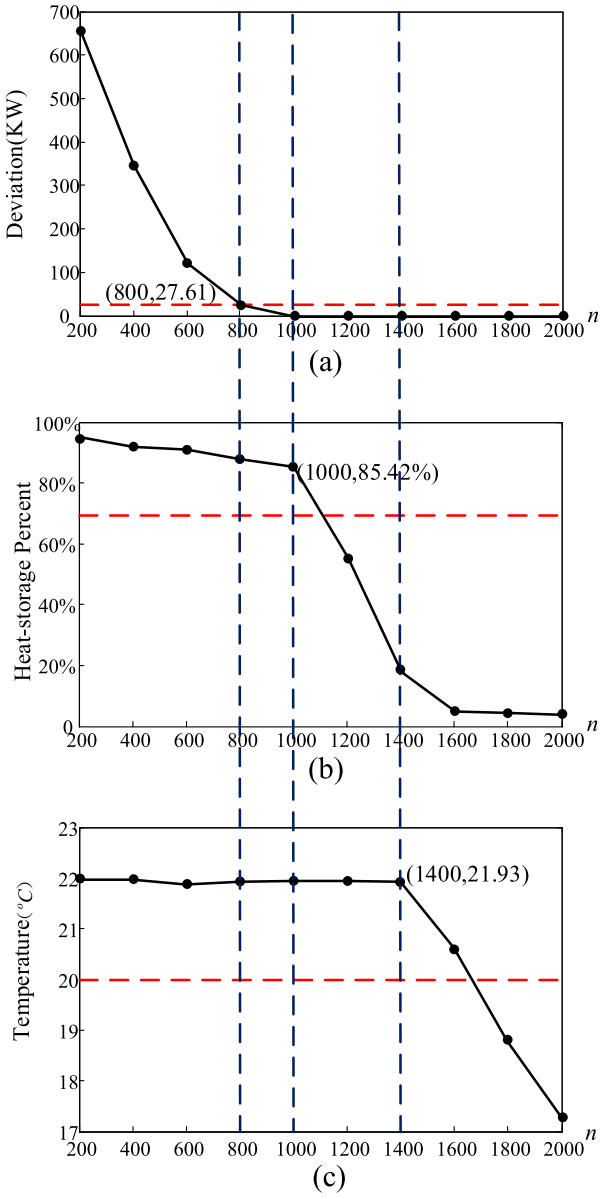

FIGURE 14. Evolution of three performances with increasing numbers of REHs. (a) Accommodation deviation. (b) Heat-storage percent. (c) Temperature.

and heat-storage percent, but still a large deviation. When n is in (800,1000], the deviation is lower than 5% and eventually converges to 0 with ideal temperature and heat-storage percent, which results from the approximate balance between demands and response. Particularly, since the data of temperature and heat-storage percent are from instantaneous status of REHs, the target response can only support partial REHs to achieve ideal temperature at the final slot, and others are at the heat-exothermic state, which causes smooth decrease of heat-storage percent. When n is in (1000,1400], residential demand starts to exceed the target response with increasing REHs. With the preferential consideration of temperature, heat-storage percent has a continuous drop at heat-exothermic state. When n is larger than 1400, target response is serious insufficient to meet the basic comfort demand, the temperature performance presents an obvious decline and rare heat-storage can be remained.

Comprehensively, under the given parameter settings in this paper, the aggregated loads achieve appropriate performances in the range of (800,1000]. To make a further discussion in detail, if residents participate in services such as non-real-time demand response, the number closes to 800 will be more suitable to meet the system demand with considerable residential thermal performance and lower costs. While the number closes to 1000 will be more suitable for the scenario requiring more accurate match, such as emergency demand response and real-time direct load control.

In terms of the universality of the proposed strategy, under an arbitrary and certain response curve, there always has an evolution from insufficient, balance to redundant between energy for saturating heat-storage and thermal heating of all residents and target response. Therefore, the variation tendency between performances and n is consistent with the above analysis: an appropriate number range of REHs corresponding to the evolution tendency between the numbers of REHs and response curve exists necessarily, in which system and residential demands can meet the requirements.

In summary, under different target responses, selecting an appropriate number range of the REHs contributes to realize real-time energy balance and ensure residential comfort based on analysis of residential demands and performances.

D. DISCUSSION OF SIMULATION RESULTS

According to the simulation results, it is proved that the proposed control strategy not only can balance real-time energy effectively, but also can ensure residential comfort and fairness, which is shown in better indoor temperature distribution and the heat-storage percent distribution.

Besides, the simulation results support the statement that an appropriate number range of REHs could be predicted to match the response accurately and meet residential requirements under various response curves, which is meaningful in designing a system. The accuracy of this range can be further improved by more advanced technology in the future.

VI. CONCLUSIONS

This paper presents an information control model of a single REH, and designs a collaborative fuzzy control strategy of aggregated REHs to accommodate renewable energy, which includes four processes of state awareness, real-time analysis, scientific decision-making, and precise execution. By performing and evaluating several simulations from the accommodation deviation, indoor temperature, and heat-storage percent, we demonstrate the effectiveness and advantages of the proposed strategy. The performances prove that this strategy can meet the demand of accommodating renewable energy accurately while residential requirements are satisfied.

REFERENCES

[1] J. H. Yoon, R. Baldick, and A. Novoselac, "Dynamic demand response controller based on real-time retail price for residential buildings," *IEEE Trans. Smart Grid*, vol. 5, no. 1, pp. 121–129, Jan. 2014.

[2] H. Yang, T. Xiong, and J. Qiu, "Optimal operation of DES/CCHP based regional multi-energy prosumer with demand response," *Appl. Energy*, vol. 167, pp. 353–365, Apr. 2016.

[3] M. A. Hannan *et al.*, "A review of Internet of energy based building energy management systems: Issues and recommendations," *IEEE Access*, vol. 6, pp. 38997–39014, Jul. 2018.

[4] Y. Wang *et al.*, "Energy management of smart micro-grid with response loads and distributed generation considering demand response," *J. Cleaner Prod.*, vol. 197, pp. 1069–1083, Oct. 2018.

[5] M. J. Salehpour and S. M. M. Tafreshi, "The effect of price responsive loads uncertainty on the risk-constrained optimal operation of a smart micro-grid," *Int. J. Elect. Power Energy Syst.*, vol. 106, pp. 546–560, Mar. 2019.

[6] N. Wu and H. Wang, "Deep learning adaptive dynamic programming for real time energy management and control strategy of micro-grid," *J. Cleaner Prod.*, vol. 204, pp. 1169–1177, Dec. 2018.

[7] A. Nouri, H. Khodaei, A. Darvishan, S. Sharifian, and N. Ghadimi, "RETRACTED: Optimal performance of fuel cell-CHP-battery based micro-grid under real-time energy management: An epsilon constraint method and fuzzy satisfying approach," *Energy*, vol. 159, pp. 121–133, Sep. 2018.

[8] H. Hosseinnia and B. Tousi, "Optimal operation of DG-based micro grid (MG) by considering demand response program (DRP)," *Electr. Power Syst. Res.*, vol. 167, pp. 252–260, Feb. 2019.

[9] S. A. Pourmousavi, S. N. Patrick, and M. H. Nehrir, "Real-time demand response through aggregate electric water heaters for load shifting and balancing wind generation," *IEEE Trans. Smart Grid*, vol. 5, no. 2, pp. 769–778, Mar. 2017.

[10] N. H. Abu-Hamdeh and K. A. Alnefaie, "Assessment of thermal performance of PCM in latent heat storage system for different applications," *Sol. Energy*, vol. 177, pp. 317–323, Jan. 2019.

[11] J. Lizana, D. Friedrich, R. Renaldi, and R. Chacartegui, "Energy flexible building through smart demand-side management and latent heat storage," *Appl. Energy*, vol. 230, pp. 471–485, Nov. 2018.

[12] S. Seddegh, X. Wang, A. D. Henderson, and Z. Xing, "Solar domestic hot water systems using latent heat energy storage medium: A review," *Renew. Sustain. Energy Rev.*, vol. 49, pp. 517–533, Sep. 2015.

[13] B. Zalba, J. M. Marín, L. F. Cabeza, and H. Mehling, "Review on thermal energy storage with phase change: Materials, heat transfer analysis and applications," *Appl. Therm. Eng.*, vol. 23, no. 3, pp. 251–283, Feb. 2003.

[14] M. H. Rahim, A. Khalid, N. Javaid, M. Alhussein, K. Aurangzeb, and Z. A. Khan, "Energy efficient smart buildings using coordination among appliances generating large data," *IEEE Access*, vol. 6, pp. 3490–34670, Jul. 2018.

[15] S. Shao, M. Pipattanasomporn, and S. Rahman, "Development of physical-based demand response-enabled residential load models," *IEEE Trans. Power Syst.*, vol. 2, no. 2, pp. 607–614, May 2013.

[16] H. Pombeiro, M. J. Machado, and C. Silva, "Dynamic programming and genetic algorithms to control an HVAC system: Maximizing thermal comfort and minimizing cost with PV production and storage," *Sustain. Cities Soc.*, vol. 34, pp. 228–238, Oct. 2017.

[17] N. Lu, "An evaluation of the HVAC load potential for providing load balancing service," *IEEE Trans. Smart Grid*, vol. 3, no. 3, pp. 1263–1270, Sep. 2012.

[18] A. Molina A. Gabaldón, J. A. Fuentes, and C. Alvarez, "Implementation and assess-ment of physically based electrical load models: Application to direct load control residential programmers," *IEE Proc.-Gener., Transmiss. Distrib.*, vol. 150, no. 1, pp. 61–66, 2003.

[19] H. He, B. M. Sanandaji, K. Poolla, and T. L. Vincent, "Aggregate flexibility of thermostatically controlled loads," *IEEE Trans. Power Syst.*, vol. 30, no. 1, pp. 189–198, Jan. 2014.

[20] E. L. Faida, A. P. Sivkova, and T. Y. Nikonova, "Self-Adjusting air temperature control system in residential accommodation with electric heating," in *Proc. Int. Conf. Ind. Eng., Appl. Manuf.*, 2017, pp. 1–4.

[21] C. D. Pero and N. HalimePaksoy, "Energy storage key performance indicators for building application," *Sustain. Cities Soc.*, vol. 40, pp. 54–65, Jul. 2018.

[22] Y. Li, J. Zhou, E. Long, and X. Meng, "Experimental study on thermal performance improvement of building envelopes by integrating with phase change material in an intermittently heated room," *Sustain. Cities Soc.*, vol. 38, pp. 607–615, Apr. 2018.

[23] S. Teleke, M. E. Baran, A. Q. Huang, S. Bhattacharya, and L. Anderson, "Control strategies for battery energy storage for wind farm dispatching," *IEEE Trans. Energy Convers.*, vol. 24, no. 3, pp. 725–732, Sep. 2009.

[24] S. Teleke, M. E. Baran, S. Bhattacharya, and A. Q. Huang, "Rule-based control of battery energy storage for dispatching intermittent renewable sources," *IEEE Trans. Sustain. Energy*, vol. 1, no. 3, pp. 117–124, Oct. 2010.

[25] T. K. A. Brekken, A. Yokochi, A. von Jouanne, Z. Z. Yen, H. M. Hapke, and D. A. Halamay, "Optimal energy storage sizing and control for wind power applications," *IEEE Trans. Sustain. Energy*, vol. 2, no. 1, pp. 69–77, Jan. 2011.

[26] D. Gayme and U. Topcu, "Optimal power flow with large-scale storage integration," *IEEE Trans. Power Syst.*, vol. 28, no. 2, pp. 709–717, May 2013.

[27] C. Wang, Z. Lu, and Y. Qiao, "A consideration of the wind power benefits in day-ahead scheduling of wind-coal intensive power systems," *IEEE Trans. Power Syst.*, vol. 28, no. 1, pp. 236–245, Feb. 2013.

[28] D. S. Callaway, "Tapping the energy storage potential in electric loads to deliver load following and regulation, with application to wind energy," *Energy Convers. Manage.*, vol. 50, no. 5, pp. 1389–1400, May 2009.

[29] L. C. Totu, R. Wisniewski, and J. Leth, "Demand response of a TCL population using switching-rate actuation," *IEEE Trans. Control Syst. Technol.*, vol. 25, no. 5, pp. 1537–1551, Sep. 2017.

[30] L. Zeng, Y. Sun, Q. Ye, B. Qi, and B. Li, "A centralized demand response control strategy for domestic electric water heater group based on appliance cloud platform," *IEEE Trans. Power Syst.*, vol. 12, no. S2, pp. S16–S22, Dec. 2017.

[31] L. Zeng, Y. Sun, B. Li, and B. Qi, "Load control at users' demand side in cyber-physical system for balancing variable renewable generation," *IEEJ Trans. Elect. Electron. Eng.*, vol. 13, no. 12, pp. 1727–1737, Dec. 2018.

[32] L. Zeng, Y. Sun, X. Zhou, B. Li, and B. Qi, "Demand dispatch in cyber-physical load aggregation system with multilevel incentives," *J. Modern Power Syst. Clean Energy*, vol. 6, no. 5, pp. 968–978, Sep. 2018.

[33] N. Lu and D. P. Chassin, "A state-queueing model of thermostatically controlled appliances," *IEEE Trans. Power Syst.*, vol. 19, no. 3, pp. 1666–1673, Aug. 2004.

[34] Y. Zhou, C. Wang, J. Wu, J. Wang, M. Cheng, and G. Li, "Optimal scheduling of aggregated thermostatically controlled loads with renewable generation in the intraday electricity market," *Appl. Energy*, vol. 188, pp. 456–465, Feb. 2017.

[35] M. H. Nehrir, R. Jia, D. A. Pierre, and D. J. Hammerstrom, "Power management of aggregate electric water heater loads by voltage control," in *Proc. IEEE Power Eng. Soc. Gen. Meeting*, Jun. 2007, pp. 1–6.

[36] T. Masuta and A. Yokoyama, "Supplementary load frequency control by use of a number of both electric vehicles and heat pump water heaters," *IEEE Trans. Smart Grid*, vol. 3, no. 3, pp. 1253–1262, Sep. 2012.

[37] R. Tang, S. Wang, and C. Yan, "A direct load control strategy of centralized air-conditioning systems for building fast demand response to urgent requests of smart grids," *Sustain. Cities Soc.*, vol. 87, pp. 74–83, Mar. 2018.

[38] X. Dou *et al.*, "A load-storage integrated control strategy to improve power regulation performance in a microgrid," *J. Energy Storage*, vol. 13, pp. 233–243, Oct. 2017.

[39] D. Wang, R. Zeng, and Y. Mu, "An optimization method for new energy utilization using thermostatically controlled appliances," *Power Syst. Technol.*, vol. 39, no. 12, pp. 3457–3462, Dec. 2015.

[40] D. Wang, S. Parkinson, W. Miao, H. Jia, C. Crawford, and N. Djilali, "Online voltage security assessment considering comfort-constrained demand response control of distributed heat pump systems," *Appl. Energy*, vol. 96, pp. 104–114, Aug. 2012.

[41] R. Sharma, "Lyapunov theory based stable Markov game fuzzy control for non-linear systems," *Eng. Appl. Artif. Intell.*, vol. 55, pp. 119–127, Oct. 2016.

[42] M. Begnini, D. W. Bertol, and N. A. Martins, "A robust adaptive fuzzy variable structure tracking control for the wheeled mobile robot: Simulation and experimental results," *Control Eng. Pract.*, vol. 64, pp. 27–43, Jul. 2017.

[43] H. Kakigano, Y. Miura, and T. Ise, "Distribution voltage control for DC microgrids using fuzzy control and gain-scheduling technique," *IEEE Trans. Power Electron.*, vol. 28, no. 5, pp. 2246–2258, May 2013.

[44] Y.-K. Chen, Y.-C. Wu, C.-C. Song, and Y.-S. Chen, "Design and implementation of energy management system with fuzzy control for DC microgrid systems," *IEEE Trans. Power Electron.*, vol. 28, no. 4, pp. 1563–1570, Apr. 2013.
[45] B. N. Alajmi, K. H. Ahmed, S. J. Finney, and B. W. Williams, "Fuzzy-logic-control approach of a modified hill-climbing method for maximum power point in microgrid standalone photovoltaic system," *IEEE Trans. Power Electron.*, vol. 26, no. 4, pp. 1022–1030, Apr. 2011.
[46] C. N. Papadimitriou and N. A. Vovos, "A fuzzy control scheme for integration of DGs into a microgrid," in *Proc. IEEE Medit. Electrotech. Conf.*, Apr. 2010, pp. 872–877.
[47] A. Elmitwally and M. Rashed, "Flexible operation strategy for an isolated PV-diesel microgrid without energy storage," *IEEE Trans. Energy Convers.*, vol. 26, no. 1, pp. 235–244, Mar. 2011.
[48] R. Henríquez, G. Wenzel, D. E. Olivares, and M. Negrete-Pincetic, "Participation of demand response aggregators in electricity markets: Optimal portfolio management," *IEEE Trans. Smart Grid*, vol. 9, no. 5, pp. 4861–4871, Sep. 2018.
[49] T. Yi, C. Qian, N. Jia, Q. Wang, S. Feng, and Y. Li, "Hierarchical control strategy for residential demand response considering time-varying aggregated capacity," *Int. J. Elect. Power Energy Syst.*, vol. 97, pp. 165–173, Apr. 2018.
[50] C. Chen, J. Wang, and S. Kishore, "A distributed direct load control approach for large-scale residential demand response," *IEEE Trans. Power Syst.*, vol. 29, no. 5, pp. 2219–2228, Sep. 2014.
[51] Q. Wang, C. Zhang, Y. Ding, G. Xydis, J. Wang, and J. Østergaard, "Review of real-time electricity markets for integrating distributed energy resources and demand response," *Appl. Energy*, vol. 138, pp. 695–706, Jan. 2015.
[52] M. Motalleb and R. Ghorbani, "Non-cooperative game-theoretic model of demand response aggregator competition for selling stored energy in storage devices," *Appl. Energy*, vol. 202, pp. 581–596, Sep. 2017.
[53] J. Saez-Gallego, M. Kohansal, A. Sadeghi-Mobarakeh, and J. M. Morales, "Optimal price-energy demand bids for aggregate price-responsive loads," *IEEE Trans. Smart Grid*, vol. 9, no. 5, pp. 5005–5013, Sep. 2018.
[54] F. Elghitani and E. El-Saadany, "Smoothing net load demand variations using residential demand management," *IEEE Trans. Ind. Informat.*, vol. 15, no. 1, pp. 390–398, Jan. 2019.
[55] F. Elghitani and W. Zhuang, "Aggregating a large number of residential appliances for demand response applications," *IEEE Trans. Smart Grid*, vol. 9, no. 5, pp. 5092–5100, Sep. 2018.

TING HUANG was born in 1996. She received the B.S. degree in communication engineering from North China Electric Power University, Beijing, China, in 2018, where she is currently pursuing the M.S. degree in information and communication engineering. Her research interest includes demand-side management under the Internet in the smart grid.

YI SUN was born in 1972. He received the M.S. degree in communication and information system and the Ph.D. degree in electric information technology from North China Electric Power University (NCEPU), Beijing, China, in 2009 and 2014, respectively, where he is currently a Professor of information and communication engineering. His research interests include smart power consumption, demand response, and power system communication technology.

BIN LI was born in Beijing, China, in 1983. He received the B.S. and Ph.D. degrees from the State Key Laboratory of Information Photonic and Optical Communications (IPOC), Beijing University of Posts and Telecommunications (BUPT), in 2005 and 2010, respectively.

He was with the Wireless And Optical Networking Research Group, Bell Labs Research China. He was a joint training Doctor with Yuan Ze University (YZU), Taiwan, where he was involved in the antenna design, antenna measurement, electromagnetic scattering, and asymptotic high-frequency techniques. In 2011, he joined North China Electric Power University (NCEPU), where he is currently an Associate Professor with the Communication Technology Research Center (CTRC), School of Electric and Electronic Engineering. His research interests include hybrid optical and wireless communication networks, the next-generation Internet, and electric power communication, network routing, and signaling technology.

JIANHONG HAO received the Ph.D. degree in plasma physics from the China Academy of Engineering Physics. She is currently a Professor with North China Electric Power University. Her research interests include physics, electronic technology, and electric power communication.